Bio-Based Nanocomposites Composed of Photo-Cured Soybean-Based Resins and Supramolecular Hydroxystearic Acid Nanofibers

Mitsuhiro Shibata
Chiba Institute of Technology
Japan

1. Introduction

Most of crystalline low molecular-weight organic compounds are recrystallized on cooling from hot solution of the organic compounds in appropriate solvents. However, in some cases, the hot solution becomes gelatinous meterial on cooling, which thermo-reversibly goes back to solution on the subsequent heating process, as is shown in Fig.1. The gelation is based on the formation of fibrous network structure over the whole range of the solvent via non-covalent (supramolecular) interactions between the low molecular-weight organic molecules. The structural characteristics of the low molecular-weight gelator are as follows: the presence of multiple functional groups capable of relatively weak physical molecular interactions such as van der Waals forces, hydrogen bonding, electrostatic forces, π-π stacking, and London dispersion forces; asymmetrical, non-planar, and bulky structures which relate to the suppression of crystal packing.

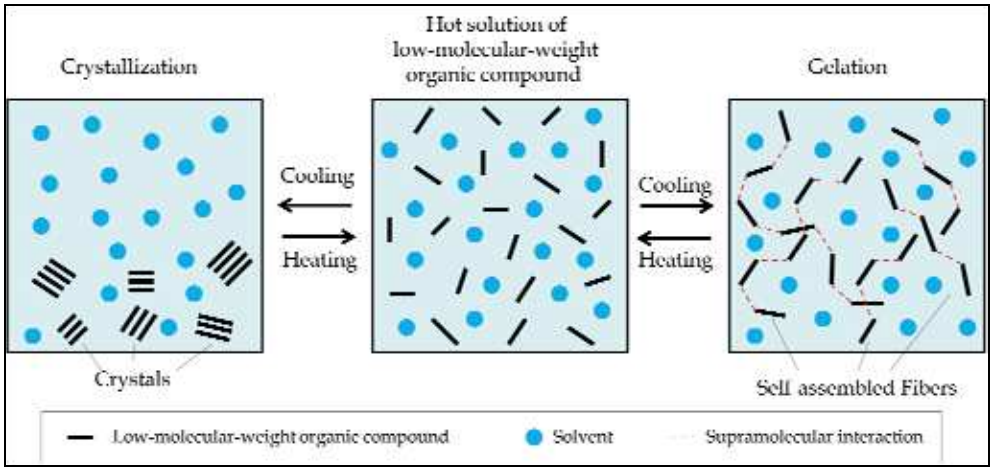

Fig. 1. Gelation and crystallization from the solution of low molecular-weight organic compound.

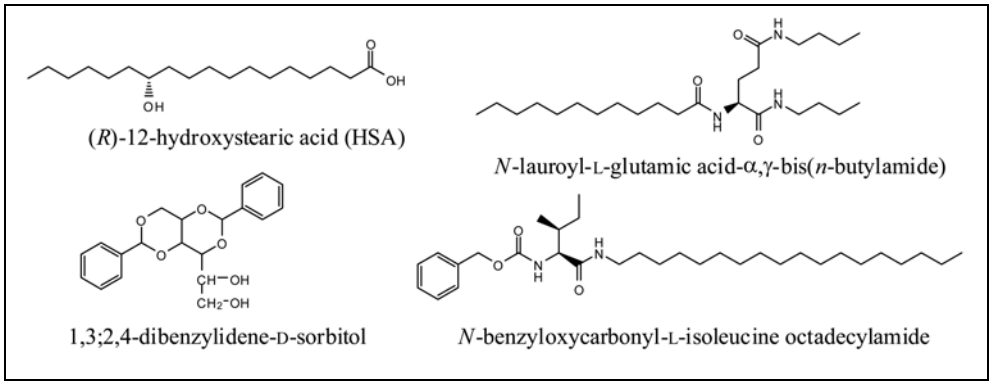

Fig. 2. Examples of various low molecular-weight organic gelators.

Up to date, a large number of low molecular-weight organic substances, such as (*R*)-12-hydroxystearic acid (HSA) (Tachibana et al., 1979, 1980; Tamura et al., 1994; Rogers & Marangoni, 2009), 1,3;2,4-dibenzylidene-D-sorbitol (Wolfe et al., 1942), and amino acid derivatives (Hanabusa et al., 1999; Hanabusa, 2005; Suzuki et al., 2006) are known to form thermo-reversible gels with supramolecular nanofibrous network in organic solvents (Fig.2). Interest in these compounds originated in the petrochemical industry to immobilize flammable solvents and to aid in the clean up of oil spills (Abdallah & Weiss, 2000; Bhattacharya & Krishnan-Ghosh, 2001). Also, HSA is industrially available organic compound which is derived from castor oil, and is used as a gelator of cooking oils (Dahlke, 1995; Rogers et al., 2008).

On the other hand, the use of renewable resources as replacement materials for industrial products is attracting great interest with increasing emphasis on environmental issues, waste disposal, and depletion of earth's limited petroleum reserves (Kaplan, 1998; Mohanty et al., 2000; Wool, 2005; Yu, 2009). Among the renewable natural resources, triglyceride plant oils represent a major class of such resources and are being used in an increasing number of industrial applications, in addition to being a food sources for human beings (Biermann et al., 2000; Güner et al., 2006; Sharma & Kundu, 2006). Soybean oil is one of the most abundant and inexpensive plant oil. Fig.3 shows the constituent fatty acid units of soybean oil and their approximate content. The major unsaturated fatty acid components of soybean oil are linoleic acid, oleic acid, and linolenic acid. It also composed of saturated fatty acids such as palmitic acid and stearic acid. The average number of C=C double bonds in the triglyceride is ca. 4.6. Unmodified soybean oil can be cationically copolymerized with styrene and divinylbenzene by use of boron trifluoride diethyl etherate to afford thermosetting resins (Li &Larock, 2001). However, the reactivity of the C=C double bonds in soybean oil is not so high that their thermal and photo-curing due to radical polymerization cannot be applied. Soybean oil can be converted to epoxidized soybean oil (ESO) and acrylated epoxidized soybean oil (AESO) with highly reactive functional groups, as is shown in Fig.4.

Bio-based epoxy resin, ESO is manufactured by the epoxidation of the double bonds of soybean oil triglycerides with hydrogen peroxide, either in formic acid or in acetic acid, and it is industrially available in large volumes at a reasonable cost (Meffert & Klush 1989; Park et al., 2004; Swern et al., 1945). It is currently mainly used as a plasticizer or stabilizer to

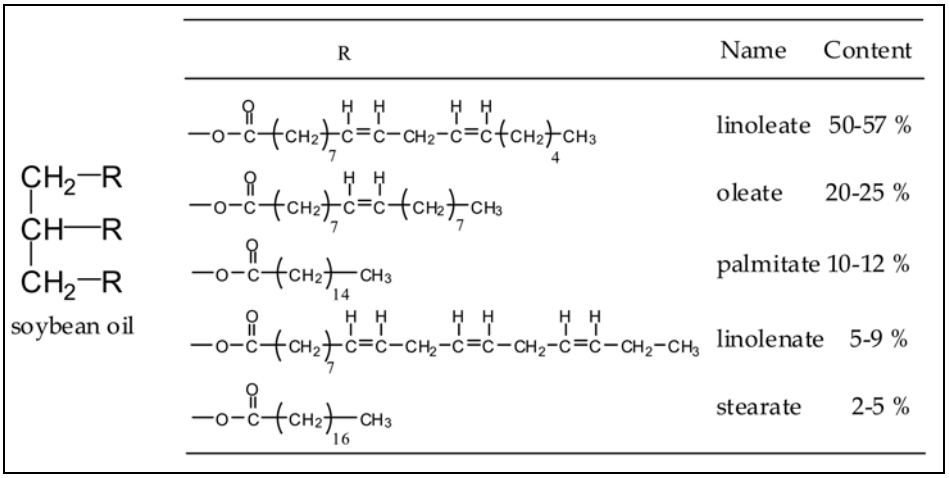

Fig. 3. Structure and fatty acid components of soybean oil.

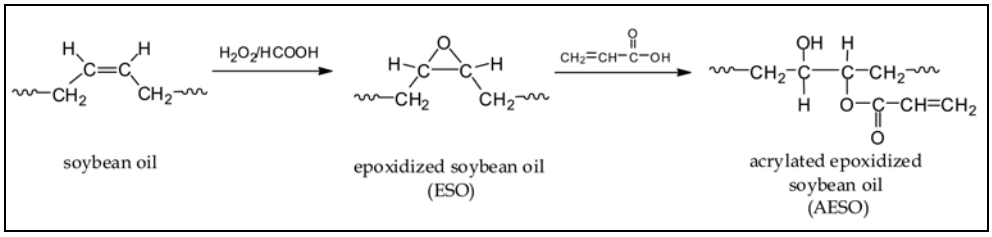

Fig. 4. Synthesis of ESO and AESO from soybean oil.

modify the properties of plastic resins such as poly(vinyl chloride) and as a reactive modifier or diluent of epoxy resin systems. Several researchers have investigated the curing and conversion of ESO into flexible, semiflexible, and rigid crosslinked resins with various approaches (Gerbase et al., 2002; Miyagawa et al., 2005; Park et al., 2004; Raghavacha, et al., 2000; Rösch & Mülhaupt, 1993; Tamami et al., 2004, Tsujimoto et al., 2003, Warth et al., 1997, Zhu et al., 2004). Bio-based acrylate resin, AESO is prepared by the reaction of ESO and acrylic acid (Khot et al., 2001). It is commercially manufactured in forms such as Ebecryl 860 (UCB Chemicals Company), and has been used extensively in the area of surface coatings. In a similar manner to general acrylate resins, AESO can be free-radically polymerized or copolymerized with reactive diluents such as styrene and methacrylic acid, to give thermosetting resins (Çolak & Küsefoğlu, 2007; Lu et al., 2005). It can be also UV-cured by use of a photoinitiator (Åkesson et al., 2010).

Recently, as environmentally benign reinforcing method of their bio-based polymers, the biocomposites with natural fibers and the nanocomposites with layered silicates have been gathering much attention. Regarding ESO-based composites, the biocomposites with kenaf, kayocell, flax, and hemp etc. have been reported by some groups (Liu et al., 2006; Tran et al., 2006; Warth et al., 1997), and the nanocomposites with organically modified layered silicates have been reported by other groups (Uyama et al., 2003; Uyama et al., 2004; Liu et al., 2005; Song et al., 2006). Also, regarding AESO-based composites, there had been some literatures

on the biocomposites of a mixture of AESO and styrene with natural fiber mats made of flax, cellulose, pulp and hemp (O'Donell et al., 2004; Khot et al., 2001), and the nanocomposites of AESO and organically modified montmorillonite (Åkesson et al., 2010; Lu et al., 2004).
If the supramolecular fibrous networks of bio-based low molecular-weight gelator are successfully formed in solid bio-based network polymer matrix, various interesting properties such as complete biodegradability and self repairing etc. are expected for the bio-based nanocomposites as compared with conventional network polymer/fiber composites. The present study describes the preparation and properties of the bio-nanocomposites composed of the ESO (Shibata et al, 2009) and AESO crosslinked by the photo-polymerization and self-assembled HSA molecules.

2. Experimental part

2.1 Materials

Epoxidized soybean oil (ESO, KAPOX S-6, oxirane oxygen 6.7%, iodine value 1.80 g-I_2/100 g) was supplied from Kao Corporation (Tokyo, Japan). Acrylated epoxidized soybean oil (AESO) was purchased from Sigma-Aldrich Japan K.K. (Tokyo, Japan). (*R*)-12-Hydroxystearic acid (HSA) was kindly supplied from Itoh Oil Chemicals Co., Ltd. (Yokkaichi, Mie, Japan). As a photoinitiator for cationic polymerization of ESO, 4-isobutylphenyl-4'-methylphenyl-iodonium hexafluorophosphate (IRGACURE® 250, Chiba Speciality Chemicals K.K. (Tokyo, Japan)) was used. Photoinitiators for radical polymerization of AESO, 1-hydroxycyclohexyl phenyl ketone (IRGACURE® 184, mp. 45-49°C, UV/VIS absorption peaks in methanol:246, 280, 333 nm) and phenyl bis(2,4,6-trimethylbenzoyl)phosphine oxide (IRGACURE® 819, mp. 127-133°C UV/VIS absorption peaks in methanol:295, 370 nm) were supplied from Chiba Specialty Chemicals K.K. (Tokyo, Japan). The structure of photo-initiators used in this study is shown in Fig.5.

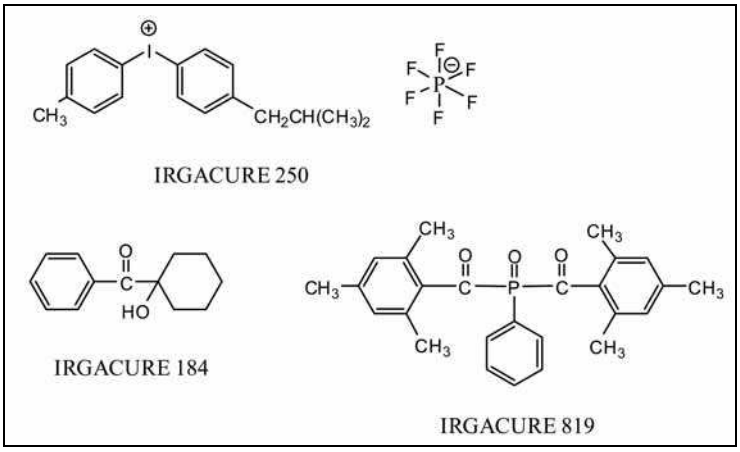

Fig. 5. Structure of photoinitiators used in this study.

2.2 Preparation of photo-cured ESO/HSA composites

A mixture of ESO 10.0 g, HSA 1.0 g, and IRGACURE® 250 0.30 g was heated to 100°C and stirred for 15 min to give a homogeneous liquid. The hot oily substance ca. 2 g was poured

on a Φ55 mm aluminum pan and was allowed to stand at room temperature to give a gelatinous material. The obtained gel was photo-irradiated under ice cooling for total 15 min at intervals of every 15 s to give a photo-cured ESO/HSA 10/1 film (thickness: *ca.* 0.8 mm). SPOT-CURE SP-7 (250 W light source, wavelength 240-440 nm, Ushio Inc., Yokohama, Japan) equipped a uniform-radiation optical unit was used for the UV curing (Irradiation distance 200 mm, Irradiation intensity 77.6 mW/cm^2). In a similar manner, the photo-cured ESO film without HSA and ESO/HSA 20/1 film were prepared.

2.3 Preparation of photo-cured AESO/HSA composites

A solution of IRGACURE® 184 0.030 g and IRGACURE® 819 0.006 g in acetone 2 mL was added to AESO 3.00 g. After the mixture was heated to 130 °C, HSA 0.300 g was added and stirred for 15 min to give a homogeneous liquid. The hot oily substance ca. 2 g was poured on a Φ55 mm aluminum pan and was allowed to stand at room temperature to give a gelatinous material. The obtained gel was photo-irradiated under ice cooling for total 5 min at intervals of every 15 s to give a photo-cured AESO/HSA 10/1 film (thickness: *ca.* 0.8 mm). SPOT-CURE SP-7 (250 W light source, wavelength 240-440 nm, Ushio Inc., Yokohama, Japan) equipped a uniform-radiation optical unit was used for the UV curing (Irradiation distance 200 mm, Irradiation intensity 77.6 mW/cm^2). In a similar manner, the photo-cured AESO film without HSA and AESO/HSA 20/1 film were prepared.

2.4 Measurements

Fourier transform infrared (FT-IR) spectra were recorded on a Shimadzu FT-IR 8100 by the attenuated total reflectance (ATR) method. The differential scanning calorimetry (DSC) was performed on a Perkin-Elmer Diamond DSC in a nitrogen atmosphere at a heating rate of 10 °C/min. The 5% weight loss temperature was measured on a thermogravimetric analyzer TGA-50 (Shimadzu Co. Ltd., Kyoto, Japan) in a nitrogen atmosphere at a heating rate of 20 °C/min. Dynamic mechanical analysis (DMA) of the rectangular films (length 35 mm, width 7 mm, thickness 0.8 mm) was performed on a Rheolograph Solid (Toyo Seiki Co., Ltd, Tokyo, Japan) with a chuck distance of 20 mm, a frequency of 1 Hz and a heating rate of 2 °C/min. Tensile and flexural tests of the rectangular films (length 35 mm, width 5 mm, thickness 0.8 mm) were performed at 20 °C using an Autograph EZ-S (Shimadzu Co. Ltd., Kyoto, Japan). Span length was 20 and 30 mm and the testing speed was 5 and 1 mm/min for tensile and flexural tests, respectively. Five specimens were tested for each set of samples, and the mean values and the standard deviation (σ) were calculated. Transmission electron microscopy (TEM) was performed on a Hitachi H-500 electron microscope with a 75 kV accelerating voltage. The films were sectioned into roughly 120 nm thin sections at –70 °C using an ultramicrotome with a diamond knife and then mounted on 200 mesh copper grids. Polarized and normal optical microscopy was performed on an Olympus BXP microscope equipped with crossed polars, a Sony CCD-IRIS color video camera interfaced to a computer, and a Japan High-tech hot-stage RH-350.

3. Characterization of composites

3.1 Characterization of photo-cured ESO/HSA composites

The mixtures of ESO/HSA (10/1 and 20/1) containing a photo-initiator, which were homogeneous liquid at 100 °C became gelatinous materials when cooled to room

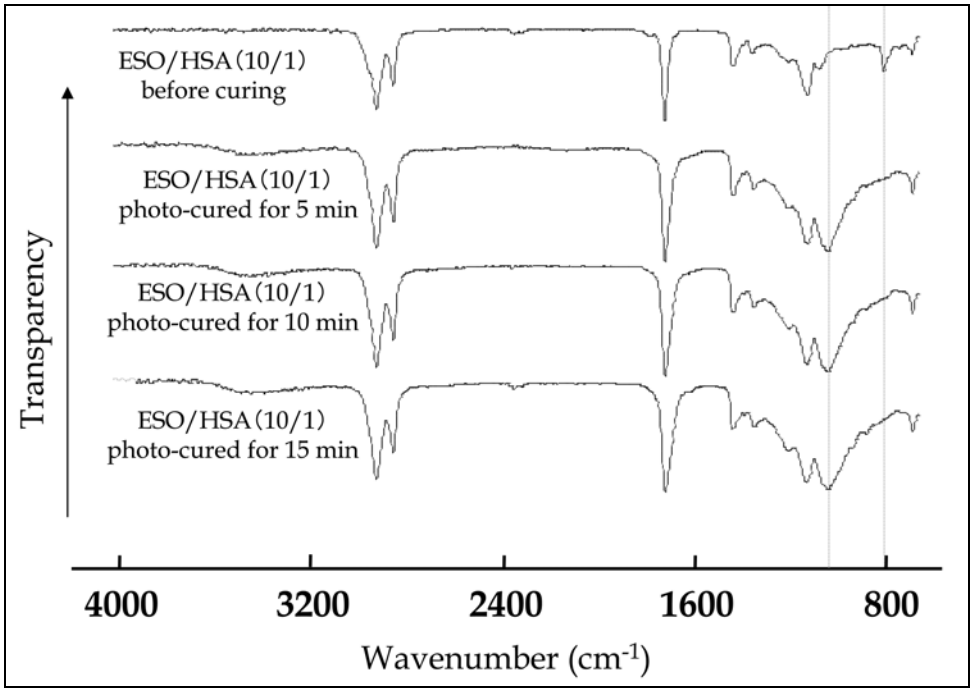

Fig. 6. FT-IR spectra of ESO/HSA(10/1) during the photo-irradiation.

temperature. Fig. 6 shows the FT-IR spectra of ESO/HSA(10/1) samples during the photo-irradiation. The ESO/HSA before curing showed an absorption peak at 800 cm^{-1} which is ascribed to anti-symmetrical stretching of epoxy ring, suggesting HSA did not react with ESO during the heating at 100 °C. On the other hand, the absorption peak characteristic to epoxy ring disappeared for the ESO/HSA photo-cured for 5 min, and a broad absorption peak at around 1100 cm^{-1} which is ascribed to the anti-symmetrical stretching vibration of C-O-C formed by the epoxy-ring opening, suggesting that photo-cationic polymerization of ESO smoothly proceeded during the photo-irradiation. The IR spectra of the ESO/HSA samples photo-cured for 10 and 15 min were almost unchanged when compared with that of the sample photo-cured for 5 min. The photo-initiated cationic polymerization is thought to be almost completed by the photo-irradiation for 5 min.

Fig. 7 shows the first heating DSC thermograms of ESO and ESO/HSA(10/1) samples containing a photo-initiator before and after the photo-irradiation for 15 min. The ESO before curing showed multiple endothermic peaks between -66 and -9 °C, indicating that ESO is a mixture of several crystalline epoxidized triglycerides. However, the photo-cured ESO had no endothermic peak, suggesting that the crystallization is inhibited by the crosslinking of epoxy groups of ESO. The gelatinous ESO/HSA(10/1) before curing had multiple melting peaks of the ESO component around -63~-3 °C and a thermal transition at 56.7 °C with ΔH = 19.9 J/g-HSA. The temperature and enthalpy change of the thermal transition were considerably lower than T_m 77.7 °C and ΔH_m 159 J/g-HSA of crystalline HSA, indicating that the thermal change is not due to melting of crystalline but due to isotropization of the mesophase composed of nano-fibrillar HSA aggregates. The reason

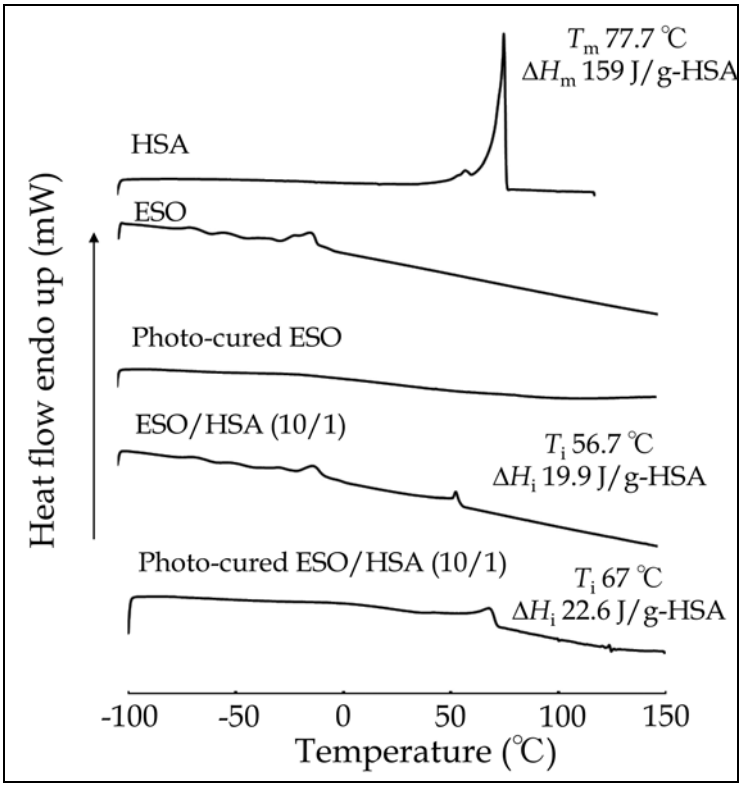

Fig. 7. The first heating DSC thermograms of HSA and the ESO and ESO/HSA(10/1) samples containing a photo-initiator before and after the photo-irradiation for 15 min. Reprinted from Shibata et al. (2009) with permission of John Wiley & Sons Inc.

why the enthalpy change is much smaller should be attributed to the fact that the mesophase is thermodynamically unstable when compared to the perfect crystal. Also, in the case of nanofibers with tiny dimensions, the free surface energy plays an important role and decreases the measured enthalpy change of the nano-fibrillar aggregates. The photo-cured ESO/HSA(10/1) showed only a broad transition around 67 °C (ΔH =22.6 J/g-HSA). The fact that the enthalpy change does not decrease compared with the value before curing indicates that the supramolecular aggregation of HSA does not collapse. The broadening of the transition curve and shift to a higher temperature region suggest that the HSA supramolecular aggregates are restricted by the ESO crosslinked structure and changes to a more aggregated structure. In addition, the disappearance of the endothermic peak around -70~0 °C suggests the occurrence of the crosslinking reaction of ESO component in a similar manner to the photo-cured ESO.

Fig. 8 shows TEM images of the ESO/HSA(10/1) cured for 15 min. In the photograph of a lower magnification, dendritic aggregates of HSA were appeared in the cured ESO matrix. In the photograph of a higher magnification, it is obvious that the aggregates are composed of numerous nanofibers. It was confirmed by the DSC and TEM observations that the photo-cured ESO/HSA is a bio-based nanocomposite.

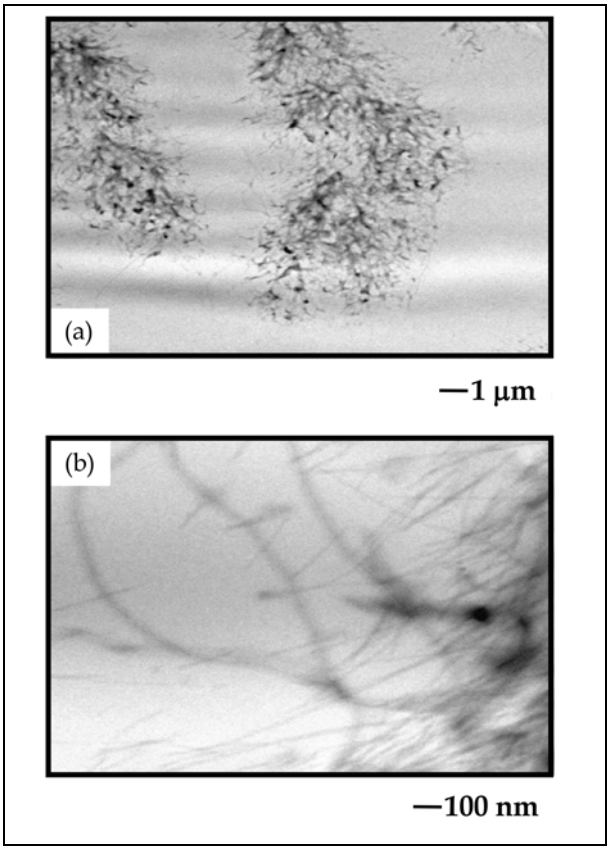

Fig. 8. TEM images of the ESO/HSA(10/1) cured for 15 min:(a) lower magnification and (b) higher magnification. Reprinted from Shibata et al. (2009) with permission of John Wiley & Sons Inc.

3.2 Characterization of photo-cured AESO/HSA composites

The mixtures of AESO/HSA (10/1 and 20/1) containing photo-initiators, which were homogeneous liquid at 130 °C became gelatinous materials when cooled to room temperature. Fig.9 shows FT-IR spectra of AESO/HSA(20/1) and AESO/HSA(10/1) photo-cured for 5 and 10 min. The FT-IR absorption peaks at 1408 and 810 cm^{-1} observed for AESO, which were assigned to olefinic C-H group in-plane and out-of-plane bending, almost disappeared for the photo-cured AESO/HSA, indicating that photo-polymerization of AESO smoothly proceeded.

Fig. 10 shows the first heating DSC thermograms of AESO/HSA(10/1) samples containing photo-initiators before and after the photo-irradiation for 5 min and 10 min. The gelatinous AESO/HSA(10/1) before curing had a thermal transition at 56.6 °C with ΔH = 63.8 J/g-HSA. The temperature and enthalpy change of the thermal transition were considerably lower than T_m 77.7 °C and ΔH_m 159 J/g-HSA of crystalline HSA, indicating that the thermal change is not due to melting of crystalline but due to isotropization of the mesophase

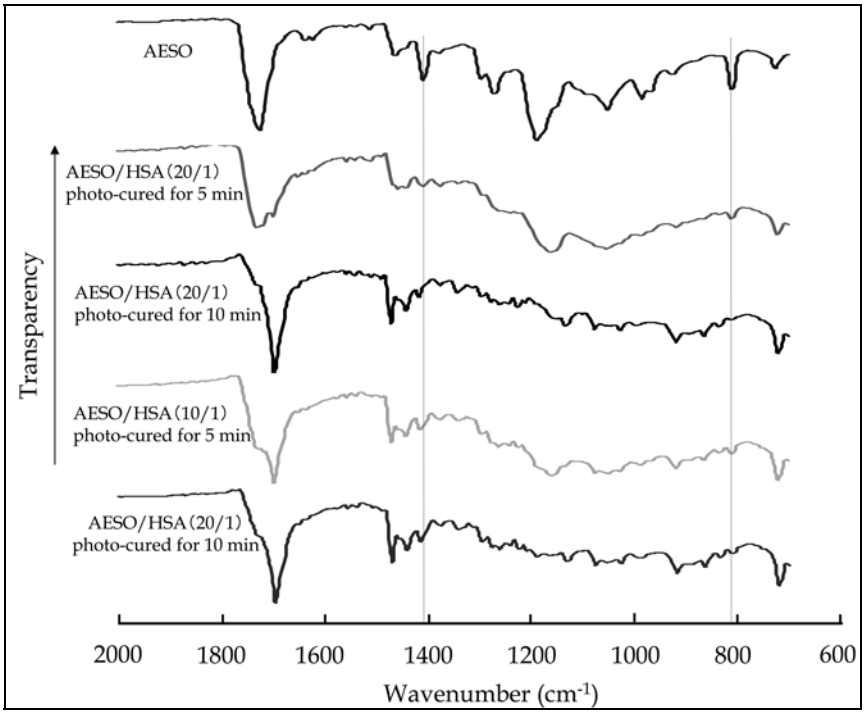

Fig. 9. FT-IR spectra of AESO and the AESO/HSA(20/1) and AESO/HSA(10/1) photo-cured for 5 and 10 min.

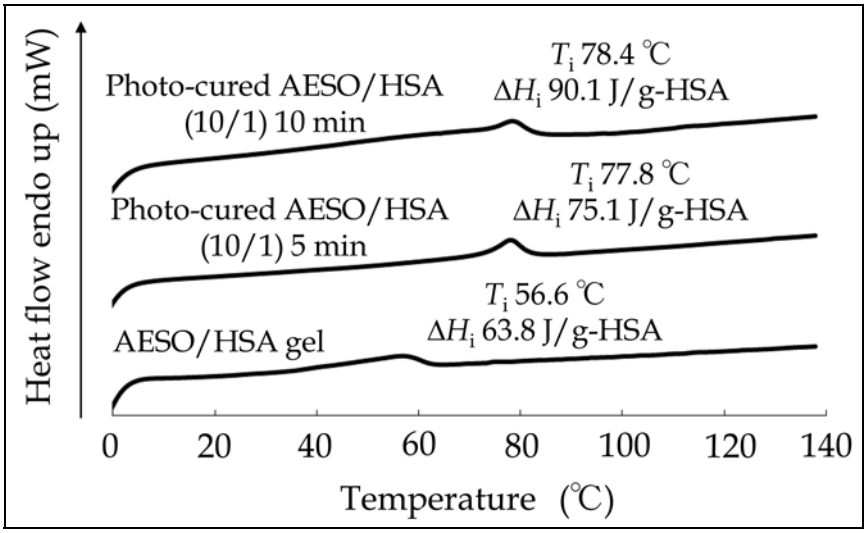

Fig. 10. The first heating DSC thermograms of AESO/HSA(10/1) containing photo-initiators before and after the photo-irradiation for 5 and 10 min.

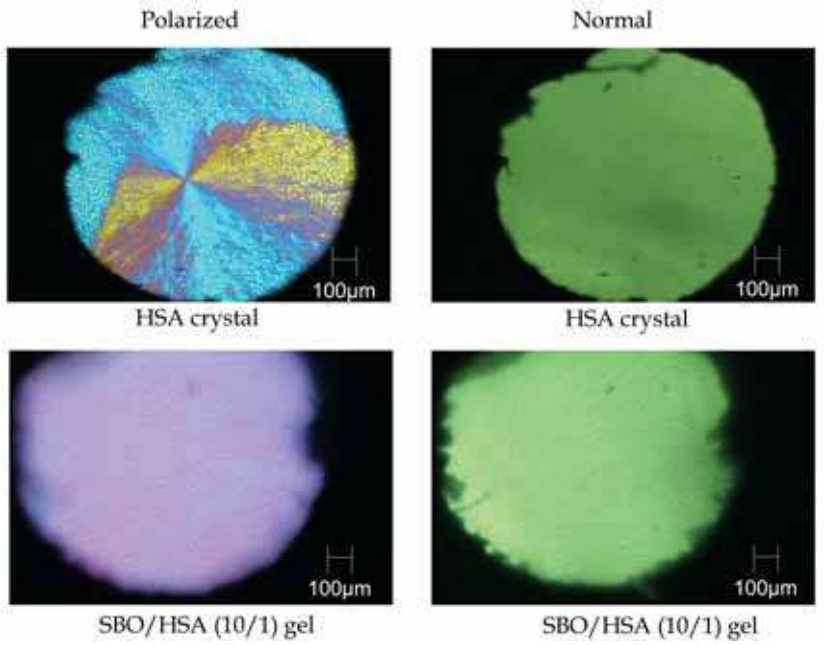

Fig. 11. Polarized and normal optical photomicrographs of HSA, SBO/HSA(10/1) gel.

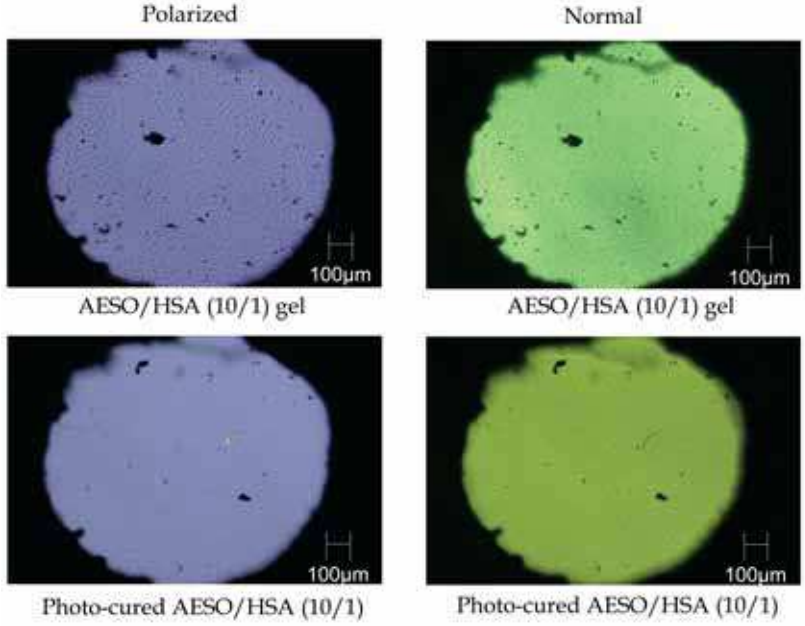

Fig. 12. Polarized and normal optical photomicrographs of AESO/HSA(10/1) gel and AESO/HSA(10/1) photo-cured for 5 min.

composed of nano-fibrillar HSA aggregates. The AESO/HSA(10/1) photo-cured for 5 min showed an endothermic peak at 77.8 °C which is higher than that before photo-curing and is almost the same as T_m of crystalline HSA. This result suggests that supramolecularly aggregated HSA molecules densely packed and changed to HSA crystalline aggregates during the photo-polymerization of AESO.

Fig.11 shows polarized and normal optical photomicrographs of HSA, soybean oil (SBO)/HSA(10/1) gel. The HSA started to crystallize at around 75 °C from the melt, and had a crystalline texture under polarized light. The formed crystals were not fibrous materials, as are obvious from the normal optical micrograph. A typical organogel of SBO/HSA10 displayed birefringence to some extent under polarized light and fibrous aggregates were formed, as are shown in the normal optical micrograph.

Fig.12 shows polarized and normal optical photo-micrographs of AESO/HSA(10/1) gel and AESO/HSA(10/1) photo-cured for 5 min. In case of AESO/HSA(10/1) gel, it is obvious that fibrous networks are homogeneously distributed in the liquid AESO. The diameter of the

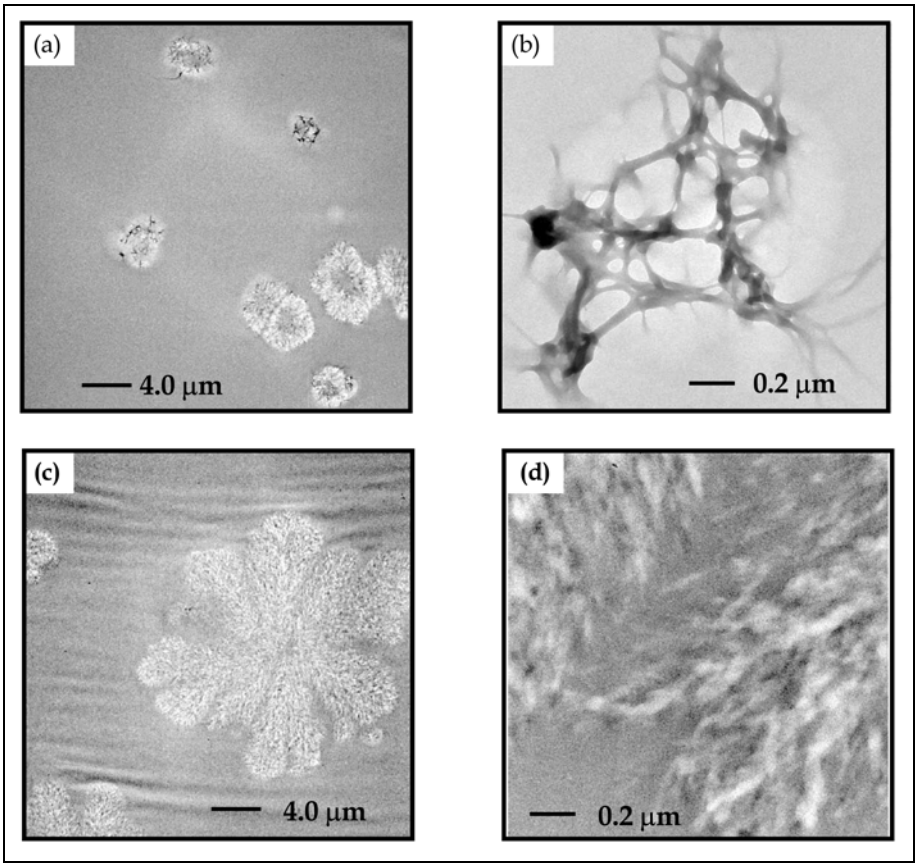

Fig. 13. TEM images of the AESO/HSA samples cured for 5 min: (a) lower magnification of AESO/HSA(20/1), (b) higher magnification of AESO/HSA(20/1) , (c) lower magnification of AESO/HSA(10/1), and (d) higher magnification of AESO/HSA(10/1).

fibrous aggregates was micro- to submicro-meters, which can be identified by optical microscope. However, most of fibrous networks disappeared for the photo-cured AESO/HSA(10/1), and some aggregated crystals was observed, indicating that the supramolecular networks changed to crystalline phase during the photo-curing of AESO.
Fig. 13 shows TEM images of the AESO/HSA(20/1) and AESO/HSA(10/1) cured for 5 min. In the photographs of a lower magnification, it is obvious that HSA crystalline aggregates are certainly formed for both the composites. It is shown from the photographs of a higher magnification that the HSA crystalline aggregates forms a network structure for AESO/HSA(20/1) and they densely packed for AESO/HSA(10/1).
The fact that photo-cured AESO/HSA has heterogeneous crystalline HSA aggregates is marked contrast to the supramolecular nano-fibrous networks of photo-cured ESO/HSA. The difference may arise from the following possibilities: the cross-linked AESO has a lower affinity with HSA than the cross-linked ESO does, and HSA molecules precipitated out from the AESO/HSA network structure.

4. Properties of composites

4.1 Mechanical properties of photo-cured ESO/HSA composites

Fig. 14 shows DMA charts of the ESO, ESO/HSA(20/1 and 10/1) photo-cured for 15 min. The tan δ peak temperature corresponding to glass transition temperature (T_g: 8.9 °C for ESO, 9.0 °C for ESO/HSA20/1, 10.4 °C for ESO/HSA10/1) little increased with increasing HSA content. In general, the addition of miscible low molecular weight compound to polymer causes a decrease of T_g due to a plasticizing effect. However, in this case, the T_g did not decrease in spite of the addition of low-molecular weight HSA. This result indicates that HSA is scarcely dissolved in the crosslinked ESO matrix, and most of HSA forms the mesophase composed of supramolecular aggregates. The storage modulus (E') at around 20~60 °C increased with increasing HSA content. The E' decreased over 60 °C due to the isotropization of the HSA nanofiber aggregates. The DMA results confirmed the nanofiber-reinforcement effect of HSA.

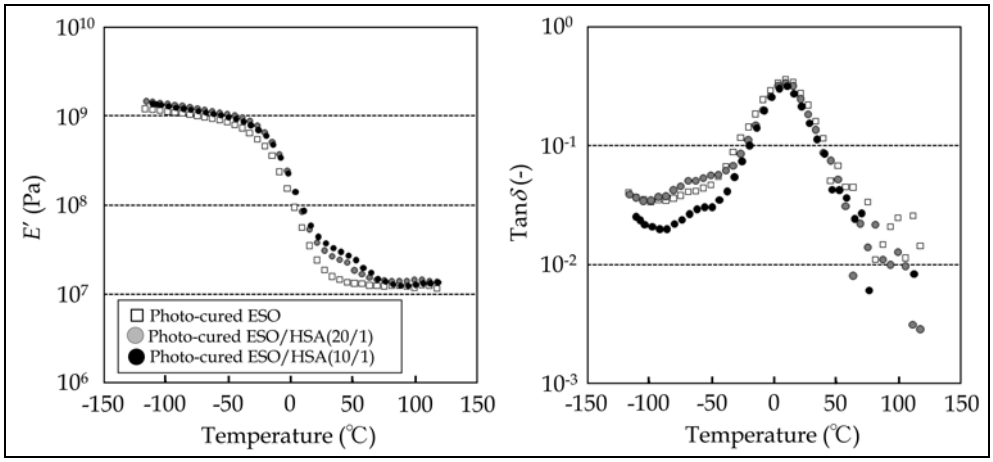

Fig. 14. DMA charts of the ESO, ESO/HSA(20/1 and 10/1) photo-cured for 15 min.
Reprinted from Shibata et al. (2009) with permission of John Wiley & Sons Inc.

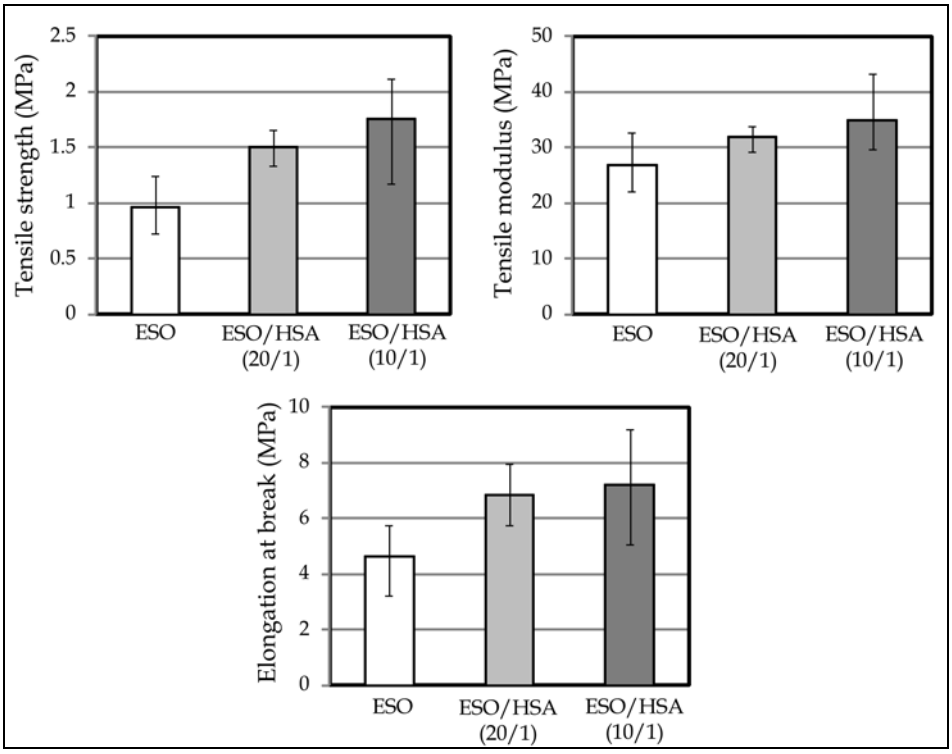

Fig. 15. Tensile properties of the photo-cured ESO/HSA nanocomposites

Fig. 15 shows the tensile properties of the photo-cured ESO/HSA nanocomposites. Tensile strength and modulus increased with increasing HSA content in agreement with the result of DMA. Although elongation at break generally did not improve in case of plant-based fiber reinforced plastics, the photo-cured ESO/HSA nanocomposites showed a little higher elongation at break than the photo-cured ESO. It may be attributed to the reasons that the supramolecular nanofiber is less rigid than plant-based fiber, and that interfacial adhesion is expected to be good because both the matrix polymer and fiber are plant oil-based organic compounds.

4.2 Mechanical properties of photo-cured AESO/HSA composites

Fig. 16 shows DMA charts of the AESO and AESO/HSA(20/1 and 10/1) photo-cured for 5 min. The tan δ peak temperature corresponding to glass transition temperature (T_g: 45.1 °C for AESO, 39.2 °C for AESO/HSA20/1, 38.1 °C for AESO/HSA10/1) decreased a little with increasing HSA content. This trend is a marked contrast with the trend of the photo-cured ESO/HSA. This result indicates that HSA is somewhat dissolved in the crosslinked AESO matrix, and most of HSA forms the crystalline phase which does not affect the molecular motion of the cross-linked AESO. The storage modulus (E') at around 70~140 °C decreased with increasing HSA content. The decrease of E' around 70 °C for photo-cured AESO/HSA(10/1) is due to the melting of the densely packed crystalline phase of HSA. A similar decrease of E' around 70 °C was not observed for photo-cured AESO/HSA(20/1),

suggesting that the melting of small amount of heterogeneously distributed HSA crystals does not affect the modulus of the whole material.

Fig. 17 shows the flexural properties of the photo-cured AESO/HSA composites. Flexural strength and modulus decreased with increasing HSA content in agreement with the result of DMA. This result indicates that the HSA crystalline phase which does not homogeneously distribute in the matrix resin does not reinforce the material. The formation of supramolecular HSA aggregates which are homogeneously distributed in the matrix is very important to get reinforced materials.

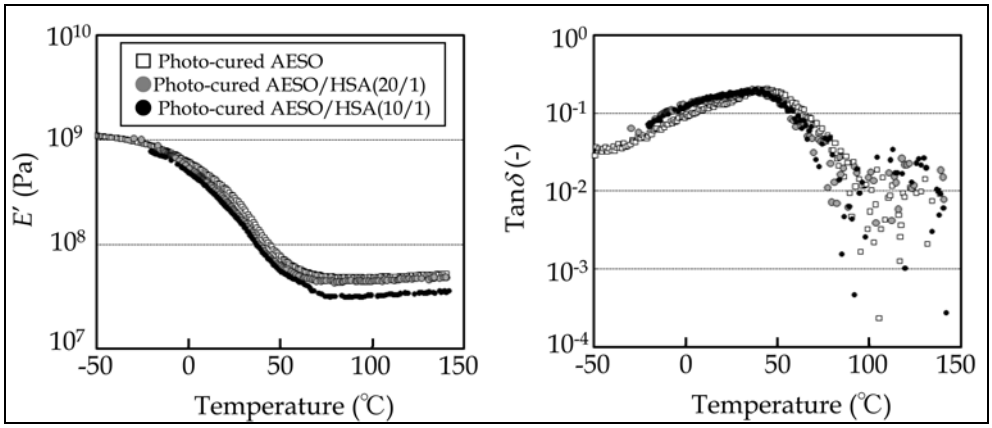

Fig. 16. DMA charts of the AESO and AESO/HSA(20/1 and 10/1) photo-cured for 5 min.

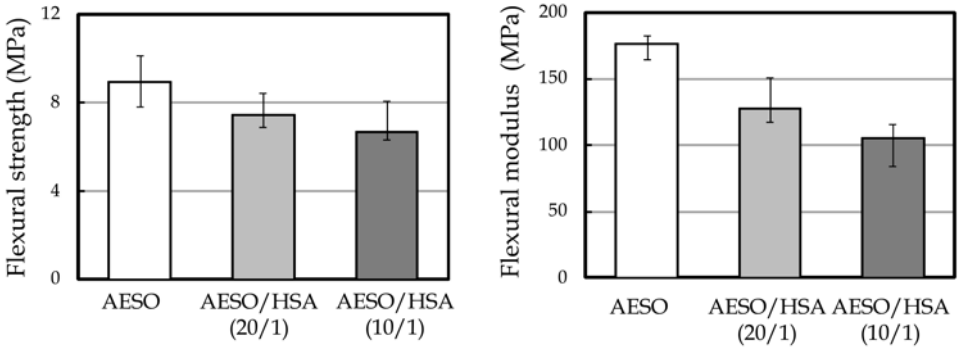

Fig. 17. Flexural properties of the photo-cured AESO/HSA composites.

4.3 Thermodegradable properties of composites

Table 1 summarizes 5 % weight loss temperature measured by TGA for the photo-cured ESO/HSA and AESO/HSA composites. The 5 % weight loss temperature of HSA itself was 276 °C, which is considerably lower than those of the photo-cured ESO and AESO. Therefore, the 5 % weight loss temperature of photo-cured ESO/HSA and AESO/HSA decreased with increasing HSA content.

Photo-cured sample	5 % weight loss temperature (°C)
ESO	374.8
ESO/HSA(20/1)	360.1
ESO/HSA(10/1)	344.4
AESO	369.2
AESO/HSA(20/1)	320.5
AESO/HSA(10/1)	303.8

Table 1. The temperature at 5 % weight loss measured by TGA for the photo-cured samples.

5. Application of this technology

This technology using cross-linked polymer can be applied to thermoplastic polymer. Recently, we reported the biocomposites of castor-oil modified poly(ε-caprolactone) (CO-PCL) and self-assembled HSA fibers (Shibata et al., 2010). The CO-PCL is synthesized by the ring-opening polymerization of ε-caprolactone (CL) initiated from the hydroxyl groups of castor oil in a feed molar ratio of CL/OH = 30/1, as is shown in Fig. 18. The degree of polymerization of ε-caprolactone unit per one segment of CO-PCL measured by ^{1}H-NMR was 29.7. After the CO-PCL was mixed with HSA at 100 °C, the mixture was gradually cooled to room temperature to give a CO-PCL/HSA composite. The abbreviation CO-PCL/HSA5, 10, and 15 means the HSA content 5, 10, and 15 phr.

In order to confirm the formation of organogel during the cooling stage of CO-PCL/HSA samples, the rheological measurement was performed. When the CO-PCL/HSA samples were cooled from 80 °C, the elastic modulus (G') of liquefied sample rapidly increased around 67-55 °C and again increased around 47-43 °C (Fig. 19). The first increase of G' is due to an increase of viscosity due to the formation of HSA organogel. The temperature at which the G' starts to rise increased with increasing content of HSA. The second increase of G' is due to the crystallization of CO-PCL. In case of CO-PCL itself, the G' rapidly rose at 39 °C due to the crystallization, indicating that the formation of HSA organogel promotes the crystallization of CO-PCL component. This is supported by the comparison of the crystallization temperature (T_c) determined from the cooling DSC thermograms of CO-PCL/HSA and CO-PCL. Thus, the T_c's of CO-PCL/HSA5, 10, and 15 samples are 32.1, 33.4, and 33.5 °C, respectively, which are higher than that of CO-PCL (15.8 °C).

Fig. 20 shows polarized and normal optical photomicrographs of CO-PCL/HSA10 during the cooling stage from 85 °C at a rate of -1 °C/min and the subsequent heating stage from 40 °C at a rate of 1°C/min. When the CO-PCL/HSA10 was cooled from 85 °C, at which the sample is isotropic liquid, fibrous network started to form at around 60 °C, and then crystallization of CO-PCL occurred. We could not clearly see the fibrous network in the normal optical photograph of 40 °C, because of the presence of CO-PCL crystals. However, when the sample was again heated at a rate of 1 °C/min from 40 °C, fibrous network could be seen at around 55 °C which is near the T_m of CO-PCL. This result shows that the fibrous network which was formed during the cooling process is not collapsed by the crystallization of CO-PCL.

Fig.21 shows the first heating DSC thermograms of the CO-PCL, CO-PCL/HSA samples annealed at 60 °C for 2 h. Melting temperature of the annealed CO-PCL was 55.2 °C, which was lower than that of as-prepared CO-PCL (60.1 °C). Since as-prepared CO-PCL was precipitated from the chloroform solution by dilution with methanol, the sample had a higher melting temperature than the annealed sample which was crystallized from the melt.

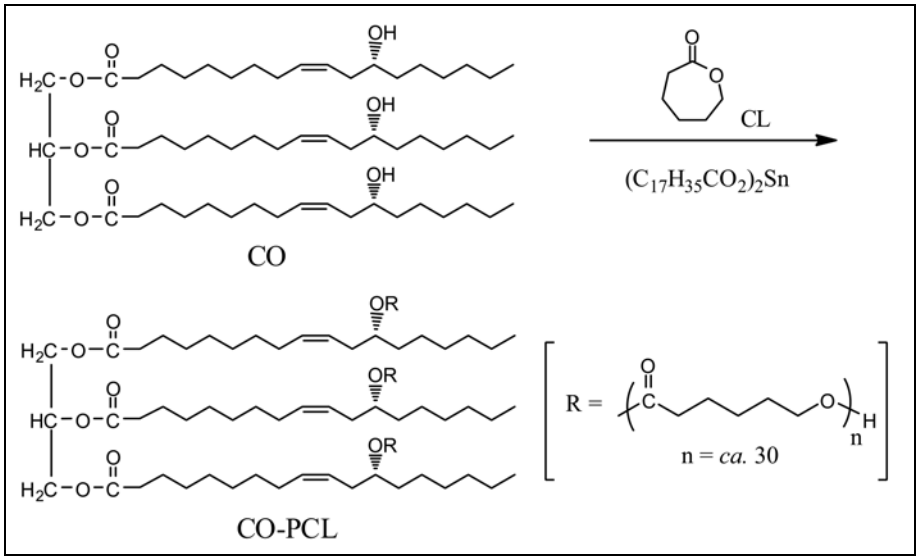

Fig. 18. Synthesis of CO-PCL. Reprinted from Shibata et al. (2010) with permission of John Wiley & Sons Inc.

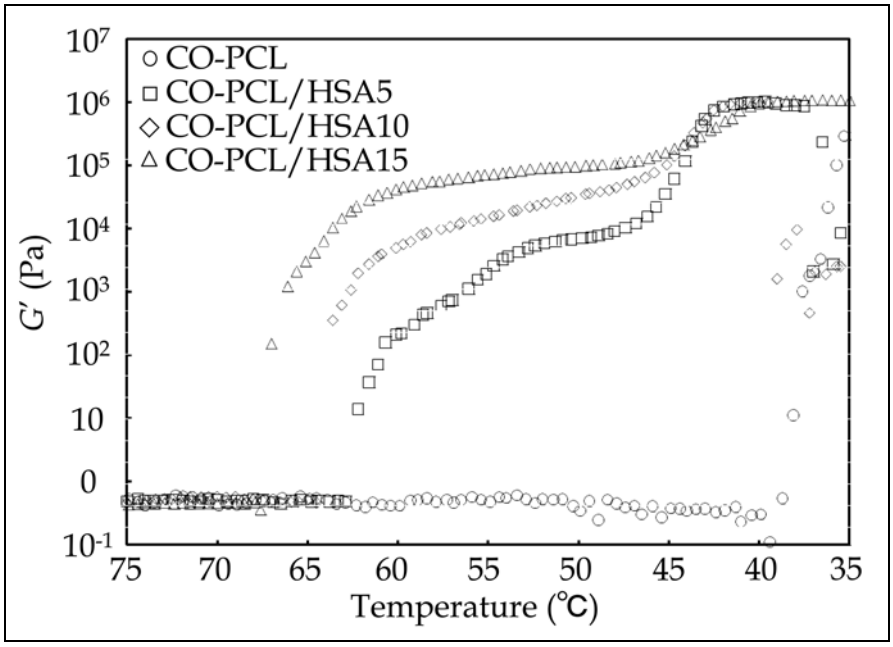

Fig. 19. Temperature dependency of G' at a cooling rate of -1 °C /min for CO-PCL, CO-PCL/HSA5, CO-PCL/HSA10, and CO-PCL/HSA15. Reprinted from Shibata et al. (2010) with permission of John Wiley & Sons Inc.

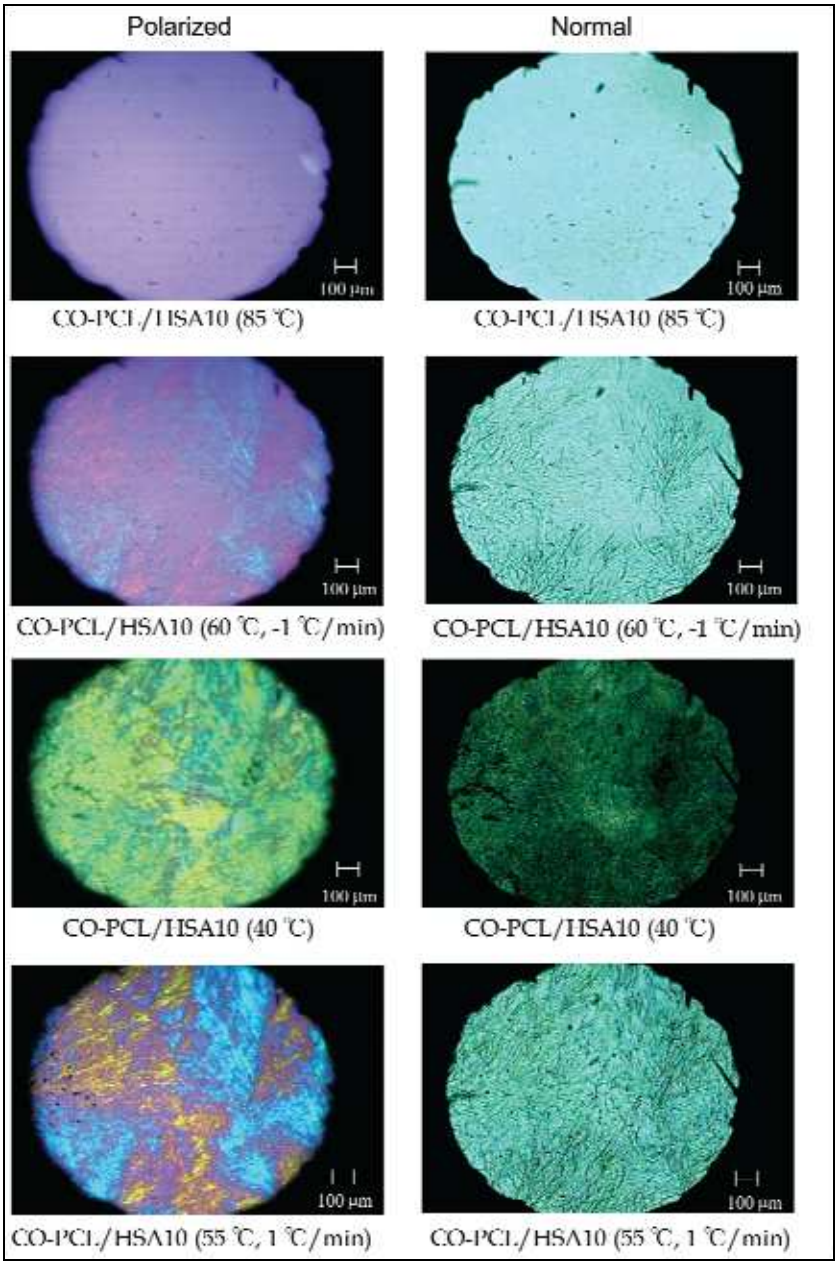

Fig. 20. Polarized and normal optical photomicrographs of CO-PCL/HSA10 samples during the cooling stage from 85 °C at a rate of -1 °C/min and the subsequent heating stage from 40 °C at a rate of 1 °C/min. Reprinted from Shibata et al. (2010) with permission of John Wiley & Sons Inc.

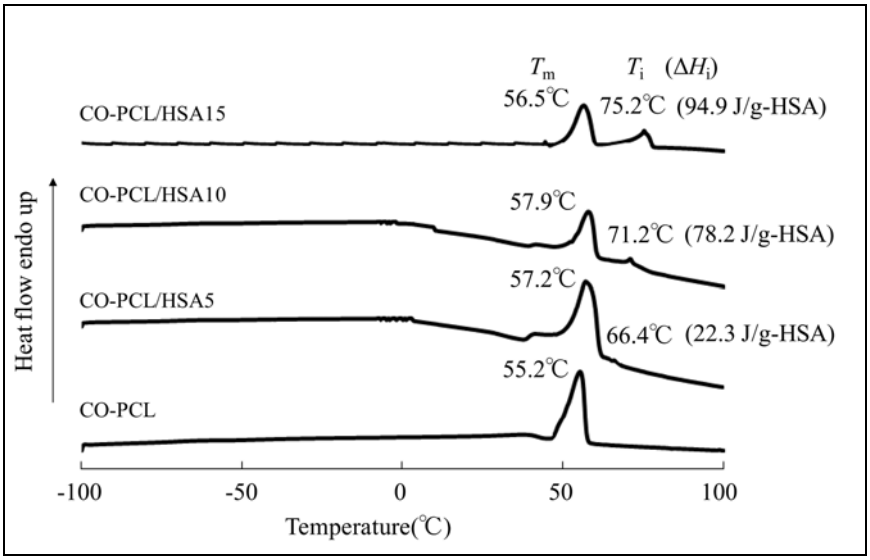

Fig. 21. The first heating DSC thermograms of the CO-PCL, CO-PCL/HSA5, CO-PCL/HSA10, and CO-PCL/HSA15 samples annealed at 60°C for 2 h. Reprinted from Shibata et al. (2010) with permission of John Wiley & Sons Inc.

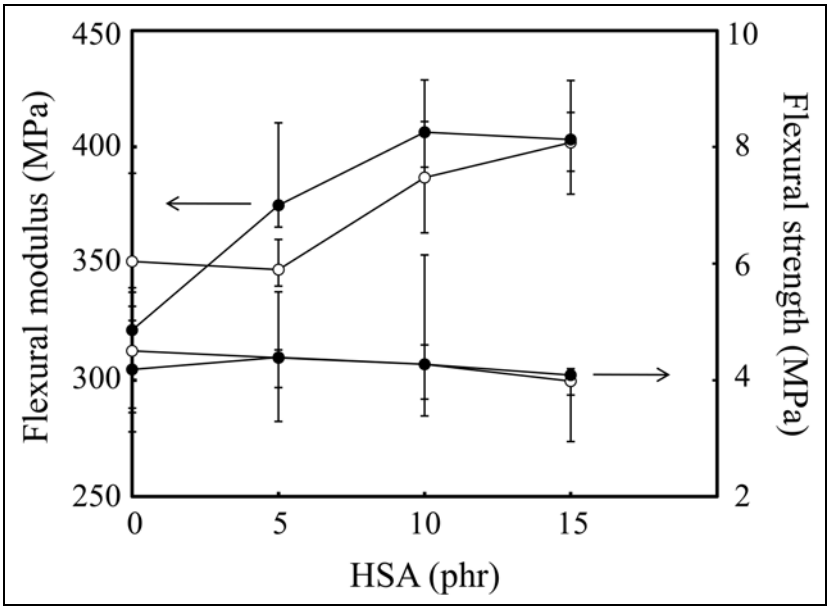

Fig. 22. Flexural properties at 25 °C for the CO-PCL/HSA samples annealed at 60 °C for 2 h (●) and without annealing (○). Reprinted from Shibata et al. (2010) with permission of John Wiley & Sons Inc.

The annealed CO-PCL/HSA5 showed a weak endothermic peak (T_i = 66.4 °C, ΔH_i = 22.3 J/g-HSA) in addition to a strong endothermic peak due to the melting of CO-PCL component (T_m = 57.2°C, ΔH_m = 55.9 J/g-HSA). The temperature of the weak peak is near the T_i of SBO/HSA10 (66.2 °C), suggesting the formation of supramolecular aggregates of HSA. The T_i and ΔH_i of CO-PCL/HSA samples increased with increasing HSA amount, suggesting the HSA supramolecular mesophase is more densely packed and gradually becomes close to crystalline phase.
Fig.22 shows flexural strength and modulus at 20°C for the CO-PCL/HSA samples annealed at 60 °C for 2 h and without annealing. For both the samples, the flexural modulus tended to increase with increasing HSA content in the range of 0-10 phr and leveled off at 15 phr. Also, the annealed CO-PCL/HSA5 and CO-PCL/HSA10 had higher flexural modulus than the corresponding samples without annealing. However, for the CO-PCL/HSA15, the effect of annealing on the increase of modulus was little. This result is in agreement with the fact that the CO-PCL/HSA15 without annealing had rather higher ΔH_i than the annealed CO-PCL/HSA15.

6. Conclusions

Bio-based nanocomposites of photo-cured ESO/HSA and AESO/HSA were prepared, and their morphologies and properties were investigated.
The DSC analysis revealed that T_i of the mesogenic HSA aggregates for the photo-cured ESO/HSA is 67 °C, which is higher than that (56.7 °C) for the ESO/HSA before curing and lower than T_m (77.7°C) of crystalline HSA. The TEM observation of the photo-cured ESO/HSA revealed that dendritic clusters of HSA nanofibers are formed in the crosslinked ESO matrix. Storage modulus, tensile modulus, and tensile strength of the photo-cured ESO/HSA increased with increasing HSA content.
In contrast to the ESO/HSA, the fibrous network of AESO/HSA gel changed to crystalline phase during the photo-curing, as is obvious from the change of T_i in the DSC thermograms and microscopic analyses. In case of the photo-cured AESO/HSA, the flexural strength and modulus decreased with increasing HSA content. This result is attributed to the fact that the formed HSA crystalline phase heterogeneously distributed in the cross-linked matrix AESO resin. The difference arises from the fact that the cross-linked AESO has a lower affinity with HSA than the cross-linked ESO does. From these observations, it was revealed that the selection of soybean-based resin with appropriate affinity to HSA is important to get a high-performance biocomposite with supramolecular HSA nanofibers.
The method established in the crosslinked ESO/HSA was applied to the bio-based thermoplastic resin, CO-PCL. As a result of the preparation of CO-PCL/HSA biocomposites, fibrous network was successfully formed in the CO-PCL matrix. The formation of fibrous network was confirmed by the normal and polarized optical microscopic analyses. The flexural and storage modulus of the CO-PCL/HSA samples increased with increasing HSA content. The CO-PCL/HSA is a new molecular composite whose mechanical recycling and self repairing is possible due to the repeated melting and self assembling of the fibrous network.
The use of renewable triglyceride plant oil as replacement materials of petroleum-based industrial materials is very important in order to save earth's limited petroleum resources and suppress global warming and environmental issues due to waste disposal. All the components (ESO, AESO, CO-PCL, and HSA) of the composites developed in this study are based on plant

oil resources. In general, plant oil-based materials have relatively poor mechanical properties because the plant oil contains long-chain fatty acid moiety. The drawback was successfully improved by the formation of supramolecular HSA fibrous network. It is expected that the biocomposites in this study are completely biodegradable materials.

7. References

Åkesson, D.; Skrifvars, M.; Lv, S.; Shi, W.; Adekunle, K.; Seppälä, J. & Turunen, M. (2010). Preparation of nanocomposites from biobased thermoset resins by UV-curing. *Progress in Organic Coatings*, Vol. 67, No. 3, pp. 281-286, ISSN: 0300-9440.

Biermann, U.; Metzger, J. O.; Friedt, W.; Luehs, W.; Lang, S.; Machmueller, G.; Schneider, M. P.; Ruesch, G. K. M. & Schaefer, H. J. (2000). New Syntheses with Oils and Fats as Renewable Raw Materials for the Chemical Industry. *Angewandte Chemie International Edition*, Vol. 39, No. 13, pp. 2206-2224, ISSN: 1433-7851.

Çolak, S. & Küsefoğlu, H. (2007). Synthesis and interfacial properties of aminosilane derivative of acrylated epoxidized soybean oil. *Journal of Applied Polymer Science*, Vol. 104, No. 4, pp.2244-2253, ISSN: 0021-8995.

Dahlke, B.; Hellbardt, S.; Paetow, M. & Zech, W. H. (1995). Polyhydroxy fatty acids and their derivatives from plant oils. *Journal of the American Oil Chemists' Society*, Vol. 72, No. 3, pp. 349-353, ISSN: 0003-021X.

Gerbase, A. E.; Petzhold, C. L. & Costa, A. P. O. (2002). Dynamic mechanical and thermal behavior of epoxy resins based on soybean oil. Journal of the American Oil Chemists' Society, Vol. 79, No. 8,pp. 797-802, ISSN: 0003-021x.

Güner, F. S.; Yağı, Y. Y. & Erciyes, A. T. (2006). Polymers from triglyceride oils. *Progress in Polymer Science*, Vol. 31, pp. 633-670, ISSN: 0079-6700.

Hanabusa, K. (2005). Development of organogelators based on supramolecular chemistry. In: *Macromolecular Nanostructured Materials (Springer Series in Materials Science)*, Ueyama, N. & Harada, A. (Ed.), pp.118-136, Kodansha Ltd., ISBN: 4-06-211242-6, Tokyo.

Hanabusa, K.; Hiratsuka, K.; Kimura, M. & Shirai, H. (1999). Easy preparation and useful character of organogel electrolytes based on low molecular weight gelator. *Chemistry of Materials*, Vol. 11, No. 3, pp. 649-655, ISSN: 0897-4756.

Kaplan, D. L. (Ed.) (1998). *Biopolymers from renewable resources*, Springer-Verlag, ISBN:3-540-63567-x, Berlin Heidelberg

Khot, S. N.; Lascala, J. J.; Can, E.; Morye, S. S.; Williams, G. I.; Palmese, G. R.; Kusefoglu, S. H. & Wool, R. P. (2001). Development and application of triglyceride-based polymers and composites. *Journal of Applied Polymer Science*, Vol. 82, No. 3, pp.703-723, ISSN: 0021-8995.

Li, F. & Larock, R. C. (2001). New soybean oil-styrene-divinylbenzene thermosetting copolymers I: Synthesis and cheacterization. *Journal of Applied Polymer Science*, Vol. 80. pp. 658-670, ISSN: 0021-8995.

Liu, Z.; Erhan, S. Z.; Akin, D. E. & Barton, F. E. (2006). "Green" composites from renewable resources: Preparation of epoxidized soybean oil and flax fiber composites. *Journal of Agricultural and Food Chemistry*, Vol. 54, No. 6, pp. 2134-2137, ISSN: 0021-8561.

Liu, Z.; Erhan, S. Z. & Xu, J. (2005). Preparation, characterization and mechanical properties of epoxidized soybean oil/clay nanocomposites. *Polymer*, Vol. 46, No. 23, pp. 10119-10127, ISSN: 0032-3861.

Lu, J.; Hong, C. K. & Wool, R. P. (2004). Bio-based nanocomposites from functionalized plant oils and layered silicate. *Journal of Polymer Science, Part B: Polymer Physics*, Vol. 42, No. 8, pp. 1441-1450, ISSN: 0887-6266.

Lu, J.; Khot, S. & Wool, R. P. (2005). New sheet molding compound resins from soybean oil. I. Synthesis and characterization. *Polymer*, Vol. 46, No. 1, pp. 71-80, ISSN: 0032-3861.

Meffert, A. & Kluth, H. (1989). Process for the preparation of modified triglycerides. *U.S. Patent, 4,886, 893*.

Miyagawa, H.; Misra, M.; Drzal, L.& Mohanty, A. K. (2005). Fracture toughness and impact strength of anhydride-cured biobased epoxy. *Polymer Engineering & Science*, Vol. 45, No. 4, pp. 487-495, ISSN: 0032-3888.

Mohanty, A. K.; Misra, M. & Hinrichsen, G. (2000). Biofibres, biodegradable polymers and biocomposites: An overview. *Macromolecular Materials & Engineering*, Vol. 276/277, pp. 1-24, ISSN: 1438-7492.

O'Donnell, A.; Dweib, M. A. & Wool, R. P. (2004). Natural fiber composites with plant oil-based resin. *Composites Scienece and Technology*, Vol. 64, No. 9, pp. 1135-1145, ISSN: 0266-3538.

Park, S.-J.; Jin, F.-L. & Lee, J.-R. (2004). Synthesis and thermal properties of epoxidized vegetable oil. *Macromolular Rapid Communications*, Vol. 25, No. 6, pp. 724-727, ISSN: 1022-1336.

Raghavachar, R.; Sarnecki, G.; Baghdachi, J. & Massingill, J. (2000). Cationic, thermally cured coatings using epoxidized soybean oil. *Journal of Coatings Technology*, Vol. 72, No. 909, pp. 125-133, ISSN: 0361-8773.

Rogers, M. A. & Marangoni, A. G. (2009). Solvent-modulated nucleation and crystallization kinetics of 12-hydroxystearic acid: A nonisothermal approach. *Langmuir*, Vol. 25, No. 15, pp. 8556-8566, ISSN:0743-7463.

Rogers, M. A.; Wright, A. & Marangoni, A. G. (2008). Crystalline stability of self-assembled fibrillar networks of 12-hydroxystearic acid in edible oils. Food Research International, Vol. 41, No. 10, pp. 1026-1034, ISSN:0963-9969.

Rösch, J. & Mülhaupt, R. (1993). Polymers from renewable resoureces: polyester resins and blends based upon anhydride-cured epoxidized soybean oil. *Polymer Bulletin*, Vol. 31, No. 6, pp. 679-685, ISSN: 0170-0839.

Sharma, V. & Kundu, P. P. (2006). Addition polymers from natural oils—A review. *Progress in Polymer Science*, Vol. 31, pp. 983-1008, ISSN: 0079-6700.

Shibata, M.; Teramoto, N. & Kaneko, K. (2010). Molecular composites composed of castor oil-modified poly(e-caprolactone) and self-assembled hydroxystearic acid fibers. *Juranl of Polymer Science, Part B: Polymer Physics*, Vol 48, No.12, pp. 1281-1289, ISSN:0887-6266.

Shibata, M.; Teramoto, N.; Someya, Y. & Suzuki, S. (2009). Bio-based nanocomposites composed of photo-cured epoxidized soybean oil and supramolecular hydroxystearic acid nanofibers. , *Juranl of Polymer Science, Part B: Polymer Physics*, Vol 47, No.7, pp. 669-673, ISSN:0887-6266.

Song, B.; Chen, W.; Liu, Z. & Erhan, S. (2006). Compressive properties of epoxidized soybean oil/clay nanocomposites. *International Jurnal of Plasticity*, Vol. 22, No. 8, pp.1549-1568, ISSN: 0749-6419.

Swern, D.; Billen, G. N.; Findley, T. W. & Scanlan, J. T. (1945). Hydroxylation of Monounsaturated Fatty Materials with Hydrogen Peroxide. *Journal of the American Chemical Society*, Vol. 67, No. 10, pp. 1786-1789, ISSN: 0002-7863.

Suzuki, M.; Sato, T.; Shirai, H. & Hanabusa, K. (2006). Powerful low-molecular-weight gelators based on L-valine and L-isoleicine with various terminal groups. *New Journal of Chemistry*, Vol. 30, pp. 1184-1191, ISSN:1144-0546.

Tachibana, T.; Mori, T. & Hori, K. (1979). New type of twisted mesophase in jellies and solid films of chiral 12-hydroxyoctadecanoic acid. *Nature*, Vol. 278, pp. 578-579, ISSN: 0028-0836.

Tachibana, T.; Mori, T. & Hori, K. (1980). Chiral mesophases of 12-hydroxyoctadecanoic acid in jelly and in the solid state. I. A new type of lyotropic mesophase in jelly with organic solvents. *Bulletin of the Chemical Society of Japan*, Vol. 53, No. 6, pp. 1714-1719, ISSN: 0009-2673.

Tamami, B.; Sohn, S. & Wilkes, G. L. (2004). Incorporation of carbon dioxide into soybean oil and subsequent preparation and studies of nonisocyanate polyurethane networks. *Journal of Applied Polymer Science*, Vol. 92. No. 2. pp. 883-891, ISSN: 0021-8995.

Tamura, T.; Suetake, T.; Ohkubo, T.& Ohbu, K. (1994). Effect of alkali metal ions on gel formation in the 12-hydroxystearic acid/soybean oil system. *Journal of the American Oil Chemists' Society*, Vol. 71, No. 8, pp. 857-861, ISSN: 0003-021X.

Tsujimoto, T.; Uyama, H. & Kobayashi, S. (2003). Green nanocomposites from renewable resources: Biodegradable plant oil-silica hybrid coatings. *Macromolular Rapid Communications*, Vol. 24, No. 12, pp. 711-714, ISSN: 1022-1336.

Tran, P.; Graiver, D. & Narayan, R. (2006). Biocomposites synthesized from chemically modified soy oil and biofibers. *Journal of Applied Polymer Science*, Vol. 102, No. 1, pp. 69-75, ISSN: 0021-8995.

Uyama, H.; Kuwabara, M.; Tsujimoto, T.; Nakano, M.; Usuki, A. & Kobayashi, S. (2003). Green nanocomposites from renewable resources: plant oil-clay hybrid materials. *Chemistry of Materials*, Vol. 15, No. 13, pp.2492-2494, ISSN: 0897-4756.

Uyama, H.; Kuwabara, M.; Tsujimoto, T.; Nakano, M.; Usuki, A. & Kobayashi, S. (2004). Organic-inorganic hybrids from renewable plant oils and clay. Macromolecular Bioscience, Vol. 4, No. 3, pp.354-360, ISSN: 0897-4756.

Warth, H.; Mülhaupt, R.; Hoffmann, B.; Lawson, S. (1997). Polyester networks based upon epoxidized and maleinated natural oils. *Angewandte Makromol eculare Chemie*, Vol. 249, No. , pp. 79-92, ISSN: 0003-3146.

Wolfe, J. K.; Hann, R. M. & Hudson, C. S. (1942). 1,2,3,4-Dibenzylidene-D-sorbitol. *Journal of the American Chemical Society*, Vol. 64, No. 7, pp. 1493-1497, ISSN: 0002-7863.

Wool, R. P. (2005). Polymers and Composite Resins From Plant Oils, In: *Bio-Based Polymers and Composites*, Wool, R. P. & Sun, X. S. (ed.), pp. 56-111, Elsevier Academic Press, ISBN: 0-12-763952-7, Burlington.

Yu, L. (Ed.) (2009). *Biodegradable Polymer Blends and Composites from Renewable Resources*. John Wiley & Sons, ISBN: 98-0-470-14683-5, Hoboken.

Zhu, J.; Chandrashekhara, K.; Flanigan, V. & Kapila, S. (2004). Curing and mechanical characterization of a soy-based epoxy resin system. *Journal of Applied Polymer Science*, Vol. 91. No. 6, pp. 3513-3518, ISSN: 0021-8995.

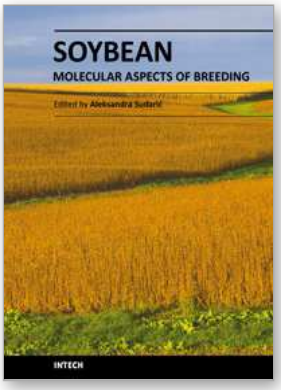

Soybean - Molecular Aspects of Breeding
Edited by Dr. Aleksandra Sudaric

ISBN 978-953-307-240-1
Hard cover, 514 pages
Publisher InTech
Published online 11, April, 2011
Published in print edition April, 2011

The book Soybean: Molecular Aspects of Breeding focuses on recent progress in our understanding of the genetics and molecular biology of soybean and provides a broad review of the subject, from genome diversity to transformation and integration of desired genes using current technologies. This book is divided into four parts (Molecular Biology and Biotechnology, Breeding for Abiotic Stress, Breeding for Biotic Stress, Recent Technology) and contains 22 chapters.

How to reference
In order to correctly reference this scholarly work, feel free to copy and paste the following:

Mitsuhiro Shibata (2011). Bio-Based Nanocomposites Composed of Photo-Cured Soybean-Based Resins and Supramolecular Hydroxystearic Acid Nanofibers, Soybean - Molecular Aspects of Breeding, Dr. Aleksandra Sudaric (Ed.), ISBN: 978-953-307-240-1, InTech, Available from: http://www.intechopen.com/books/soybean-molecular-aspects-of-breeding/bio-based-nanocomposites-composed-of-photo-cured-soybean-based-resins-and-supramolecular-hydroxystea

INTECH
open science | open minds

InTech Europe
University Campus STeP Ri
Slavka Krautzeka 83/A
51000 Rijeka, Croatia
Phone: +385 (51) 770 447
Fax: +385 (51) 686 166
www.intechopen.com

InTech China
Unit 405, Office Block, Hotel Equatorial Shanghai
No.65, Yan An Road (West), Shanghai, 200040, China
中国上海市延安西路65号上海国际贵都大饭店办公楼405单元
Phone: +86-21-62489820
Fax: +86-21-62489821